

UC Irvine

UC Irvine Previously Published Works

Title

Spatio-temporal structure of sleep slow oscillations on the electrode manifold and its relation to spindles.

Permalink

<https://escholarship.org/uc/item/3bd730n7>

Journal

Sleep, 42(1)

ISSN

0161-8105

Authors

Malerba, Paola
Whitehurst, Lauren N
Simons, Stephen B
[et al.](#)

Publication Date

2019

DOI

10.1093/sleep/zsy197

Peer reviewed



ORIGINAL ARTICLE

Spatio-temporal structure of sleep slow oscillations on the electrode manifold and its relation to spindles

Paola Malerba^{1,*}, Lauren N. Whitehurst², Stephen B. Simons³ and Sara C. Mednick¹

¹Department of Cognitive Sciences, University of California Irvine, Irvine, CA, ²Department of Psychology, University of California Riverside, Riverside, CA and ³Teledyne Scientific & Imaging, Durham, NC

*Corresponding author. Paola Malerba, Department of Cognitive Sciences, 2201 Social & Behavioral Sciences Gateway Building, University of California Irvine, Irvine, CA 92697-5100. Email: pmalerba@uci.edu.

Abstract

Electrophysiological sleep rhythms have been shown to impact human waking cognition, but their spatio-temporal dynamics are not understood. We investigated how slow oscillations (SOs; 0.5–4 Hz) are organized during a night of polysomnographically-recorded sleep, focusing on the scalp electrode manifold. We detected troughs of SOs at all electrodes independently and analyzed the concurrent SO troughs found in every other electrode within ± 400 ms. We used a k-clustering algorithm to categorize the spatial patterns of SO trough co-occurrence into three types (Global, Local or Frontal) depending on their footprint on the electrode manifold during the considered time window. When comparing the clusters across non-rapid eye movement (NREM) sleep stages, we found a relatively larger fraction of Local SOs in slow wave sleep (SWS) compared to stage 2, and larger fraction of Global SOs in stage 2 compared to SWS. The probability of SO detection in time between two electrodes showed that SO troughs of all types co-occurred at some nearby electrodes, but only Global troughs had traveling wave profiles, moving anteriorly to posteriorly. Global SOs also had larger amplitudes at frontal electrodes and stronger coupling with fast spindles (12.5–16 Hz). Indeed, SO-spindle complexes were more likely to be detected following a Global SO trough compared to SOs in other clusters. Also, the phase-amplitude modulation of SOs over spindles (modulation vector) was higher for Global SOs across the electrode manifold. Given the recent evidence of a link between thalamocortical coupling and cognition, our findings suggest stronger cognitive relevance of Global SOs as compared to other SO types in sleep memory processing.

Statement of Significance

Select brain rhythms contribute to the formation of long-term memories during sleep, including slow oscillations (SOs) in cortex, thalamic spindles, and hippocampal ripples. We introduce a novel data-driven approach to uncover the spatiotemporal profiles of events on high-density electroencephalogram (EEG) in humans, and apply it to SOs. We find three distinct types of SOs, based on topography: Global, Local, and Frontal. They differ in amplitude, spatio-temporal profiles and relation to spindles, with only Global SOs showing traveling wave profiles (anteriorly to posteriorly), larger amplitudes at frontal electrodes and stronger spindle coupling. Our findings suggest stronger cognitive relevance of Global SOs as compared to other SO types in sleep memory processing, crucial to enable sleep manipulations aimed at improving memory performance.

Clinical Trials: No clinical trial is related to this study.

Key Words: slow oscillations; local/global sleep; spindles; thalamocortical coupling

Submitted: 9 June, 2018; Revised: 6 August, 2018

© Sleep Research Society 2018. Published by Oxford University Press on behalf of the Sleep Research Society. All rights reserved. For permissions, please e-mail journals.permissions@oup.com.

Introduction

Communication between cortex and sub-cortical structures (e.g. hippocampus and thalamus) during sleep has been shown to be critical for long-term memory formation. Accordingly, select brain rhythms have been implicated in this process, particularly those found during non-rapid eye movement (NREM) sleep [1–8], including cortical slow oscillations (SOs; 0.2–1.5 Hz, lasting from a few cycles to 10 s), cortico-thalamic spindles (9–16 Hz, each event lasting 0.5–3 s), and hippocampal sharp-wave ripples (150–250 Hz, each event lasting 60–100 ms). Although the majority of these electrophysiological events are detected independently of each other, in some percentage of cases, hierarchical nesting characterizes these rhythms, where the occurrence probability of spindles is time-aligned to SO phase, and in turn the occurrence of hippocampal ripples is time-locked to phases of SOs and spindles [1, 8–11]. As coupling between these brain oscillations during sleep has been suggested to underlie transformation of recent experiences into long-term memories [12], an understanding of which events get selected to engage in thalamocortical communication is a central question in the cognitive neuroscience of memory.

SOs have been extensively studied in humans and animals [1, 13–24]. Work from Massimini et al. [17] showed that SOs dominantly travel in an anterior to posterior direction and principally emerge at frontal electrodes. However, the same study showed evidence that SOs could originate at all electrodes and travel, at least in short lengths, through a varying gradient direction. In fact, other studies showed that SOs often occur asynchronously across cortex [19, 23], and that the topography of localized SO events can be related to localized awake processing [25, 26]. This picture of a mixture of global versus local oscillatory activity during sleep is made more interesting by the proposed model by Genzel and colleagues [27] that brain processing during sleep could be mediated by different NREM mechanisms, where light sleep (stage 2 [S2]) enables global reorganization of specific learning-related connections, and deep sleep (slow wave sleep [SWS]) enables localized reorganization of connections [26, 28] via homeostatic regulation. An extension of this hypothesis would suggest that Global SOs would selectively mediate thalamocortical communication by increased coupling with brain rhythms from other brain areas, such as cortico-thalamic sleep spindles, an intriguing possibility investigated in the current study.

We investigated the global versus local aspect of brain oscillations during human sleep by examining the spatio-temporal shape of SOs on the electrode manifold using high-density electroencephalogram (EEG) and cluster analysis. We hypothesized that spatial patterns of SOs will reveal distinct clusters that contain relevant functional differences for the processes of sleep-mediated memory consolidation. We studied the patterning of SO troughs across the electrode manifold and in time, and inspired by the aforementioned hypothesis [27] that processing in NREM stages S2 and SWS is mediated by global versus local activity, we analyzed S2 and SWS separately. Furthermore, we investigated the degree of coupling of SOs and sleep spindles across our clustered groups and hypothesized that Global SOs would show greater coupling compared to other SO clusters in both sleep stages.

Methods

Sleep recordings

One night of sleep was recorded in 34 subjects (18 females). EEG data were acquired using a 32-channel cap (EASYCAP GmbH) with Ag/AgCl electrodes placed according to the international 10–20 System (Jasper, 1958). Twenty-two out of 32 electrodes were passive scalp recordings. The remaining electrodes were used for electrocardiogram (ECG), electromyogram (EMG), electrooculogram (EOG), ground, an online common reference channel (at FCz location, retained after re-referencing) and mastoid (A1 and A2) recordings. The EEG was recorded with a 1000 Hz sampling rate and was re-referenced to the contralateral mastoid (A1 and A2) post-recording. High-pass filters were set at .3 Hz and low-pass filters at 35 Hz for EEG and EOG.

Sleep scoring

Eight scalp electrodes (F3, F4, C3, C4, P3, P4, O1, and O2), the EMG and EOG were used in the scoring of the nighttime sleep data. Raw data were visually scored in 30-second epochs into wake, stage 1, stage 2 (S2), SWS, and rapid eye movement sleep (REM) according to the Rechtschaffen and Kales' (1968) manual. Note that we increased the electrode count compared to standard method to enhance scoring reliability, but did focus on the output from the C3 and C4 electrodes as well. Minutes in each sleep stage were calculated. Additionally, wake after sleep onset (WASO) was calculated as total minutes awake after the initial epoch of sleep. The outcome of scoring across all subject is reported in Supporting Data ([Supplementary Table S0](#)).

EEG analysis

All our analysis of sleep EEG data was conducted in Matlab (R2017a, The Mathworks). To produce all our topoplots, we started from code made available by Spydell et al. [29] and tailored it to our setup. To detect the presence and timing of each SO event in any given electrode, we first applied a detection algorithm which closely followed the criteria introduced by Massimini et al. [17], and was initially introduced in Dang-Vu et al. [30]. In short, the EEG signal was filtered in the 0.1–4 Hz range, and candidate portions of the signal between subsequent positive-to-negative and negative-to-positive were listed as possible SOs. These events were only considered SOs if the following criteria were satisfied: (1) the wave minimum was below or equal to 80 μ V, (2) the range of values between maximum and minimum voltage was at least 80 μ V, (3) the time between the first and second zero crossing in the data had to be between 300 ms and 1 second, and (4) the total duration of the candidate event was at most 10 seconds. The pool of candidate SO events satisfying the parameters were further screened to remove potential artifacts, by computing the amplitude at trough referenced to the average of the signal ± 10 seconds around the minimum. Events at one electrode which showed an amplitude size of 4 SDs above the mean of all events detected at that electrode were discarded, and a secondary distribution of amplitudes including all events from all electrodes of a subject was created, and again events with amplitude above 4 SDs from the mean were discarded. When

selecting the SOs happening during a given sleep stage (S2 or SWS), only SOs with beginning and end included within the sleep stage were considered. For our *spindle detection* at separate electrodes we based a detection algorithm on work by Wamsley et al. [31]. The SO and spindle detection methods were previously used in Sattari et al. [32]. Briefly, the signal underwent a continuous wavelet-transform, and its amplitude (smoothed within a 100 ms average) was compared to a threshold of four times its mean. Peaks in the amplitude signal that were above threshold were considered the peaks of spindle events, which started and ended at the times where the amplitude signal crossed the threshold. The timing of spindle peaks was used when calculating the probability of detecting spindles in relation to SO trough timing. To estimate the degree to which the sigma amplitude was modulated by the SO phase we used the modulation index (MI) as defined in Canolty et al. [33]. MIs are ideal objects when comparing samples of signal that have different lengths, because effectively they estimate how stationary in the signal is the relation between phase of one signal and amplitude of another. We use what Canolty labeled the “normalized” version of his definition of MI, where the specific MI value obtained for a phase-amplitude signal is compared to hundreds of surrogate values generated by shuffling the initial signal sample. This procedure “controls” the MI against the intrinsic extra-correlations, which could introduce an artifact in the estimate, making it a robust measure when comparing properties of signals that show different lengths. To estimate the *Sigma Amplitude Around SO troughs*, the root mean square of filtered signal at a given electrode in the sigma band (12.5–16 Hz) was computed over 100 ms-long intervals separately for each subject. The times of SO troughs detected at the same electrode during one of the two sleep stages (S2 or SWS) were listed, and the root mean square of sigma at the electrode was aligned in a peri-trough histogram (time 0 was the time of trough, and (-1, 1) seconds around the trough time was considered). This histogram (defined by subject, electrode and sleep stage) was z-scored by subtracting its mean and normalizing by its SD. For each electrode-by-sleep stage, the peri-trough histogram of z-scored sigma amplitude was averaged across all subjects, and the mean \pm SD of this signal across electrodes is shown in the left panels of Figure 6A separately for SWS and S2.

Clustering algorithm

We populated two binary matrices by listing a binary array (24 entries for 24 electrodes) for each detected SO event in a given sleep stage. Each electrode that showed an SO trough within ± 400 ms of the detected trough was marked 1 (yes) and other electrodes were marked 0 (no). Since this built a collection of binary points in a binary space, we used Hamming distance to identify (with a k-means algorithm looking for three clusters) which events were more similar versus more different. Centroids identified by the algorithm were points in the binary space, and hence had binary coordinate values. Due to the strong difference in SO count in S2 compared to SWS, it was not appropriate to cluster SOs by combining S2 and SWS events in one whole matrix. In that case, the algorithm would likely stabilize on a topographical representation closer to SWS profile and potentially hide centroids that could have been specific to S2. However, pilot clustering across all of NREM sleep revealed similar profiles of SO categories (Local, Global, and Frontal).

Results

SO density in S2 and SWS

We analyzed the night of sleep of 34 subjects, recorded with 24 channel EEG (Figure 1A). Detection of SOs was performed only during sleep epochs identified as sleep stage S2 and SWS. The detection algorithm closely followed the one described in Massimini et al. [17] except that we did not use averages across electrodes to perform an initial selection, but directly applied the detection algorithm to each electrode voltage separately (details of SO detections in Methods). One example of a detected SO trace is shown in Figure 1B, while Figure 1C shows no differences between the average of all SO traces detected in S2 and SWS. However, comparing the distribution of SO durations during the two sleep stages showed a larger tail in the S2 distribution (Supplementary Figure S1), implying that the count of SOs with longer durations was higher in S2 (the difference between the two sample distributions was statistically significant, two-sample KS test $D = 0.1308$ at a level $\alpha = 0.05$ with a sample scaling to 0.0033 rejected the null hypothesis, see Supplementary Data). As a result, the average SO frequency in S2 was lower than in SWS (average \pm SD SO period in S2: 1.2607 ± 0.5446 seconds, in SWS: 1.1119 ± 0.3762).

We compared SO density (number of detected SOs per second), and found that density in SWS was higher than in S2 for all subjects (in agreement with previous findings [17]) and in fact that density in S2 and SWS was positively correlated (Pearson’s correlation $\rho = 0.58$, $p = 0.000376 < 0.001$), as shown in Figure 1D. Given the strong correlation found, we asked if the ratio of SO density in SWS versus S2 was a constant value across the subject population by calculating its sample probability distribution (Figure 1E). If the ratio was approximately constant, the distribution should have a peak at its mean and some small variance around it, resembling a normal distribution. In our case, we found a sharp peak at the lowest values and a large positive tail, suggesting that there was no consistent ratio of SO density in SWS versus stage S2 across subjects. This implies that while all subjects showed correlated SO density in the two separate sleep stages, the specific ratio of SWS versus S2 density was not a general property of a night of sleep, but possibly a personal trait, or related to learning. Future research will be required to investigate the source of these differences. We also studied SO density in SWS and S2 separately in their topography on the electrode manifold (Figure 1F), and found that density was significantly higher in SWS compared to S2 within each electrode (Figure 1G, Wilcoxon’s paired signed-rank test with Bonferroni correction). Since previous research suggests that SO density is higher at frontal regions [19, 24], we tested the difference in density at frontal electrodes compared to other electrodes. To do that, we grouped the electrodes in Frontal, Central, Parietal, Occipital, and Left and Right (the last two for lateral electrodes), as shown in Figure 1H (left panel). The SO density at electrodes within each group was averaged separately for each subject, and S2 and SWS densities were calculated separately. Figure 1H right panel shows that SO density during SWS was highest at Frontal electrodes, significantly more than in other electrode groups, which is consistent with previous findings [17, 24].

Cluster analysis of SOs: impact of amplitude and electrode position

Together, these data were suggesting a dominant frontal trend of the SO detection on the electrode manifold. However, we

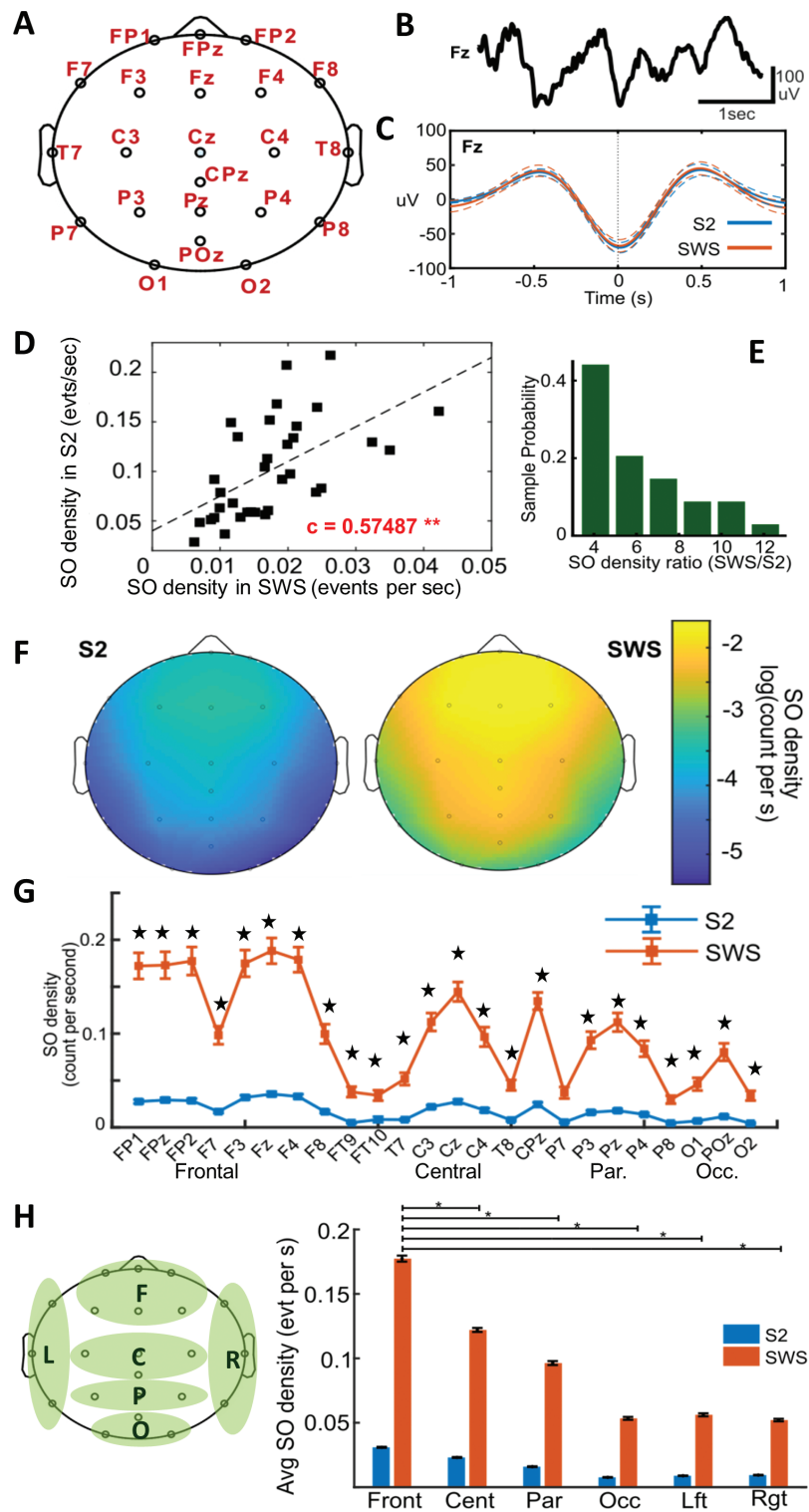


Figure 1. SO trough detection in S2 versus SWS. (A) Topoplot showing electrode placement on each subject, paired with electrode labels. (B) Example of a detected slow oscillation, trace (lasting 4 seconds) centered at the trough. (C) Average trace of SO (filtered in SO bandwidth between 0.5–1.5 Hz) around a detected trough (time = 0) shown at electrode Fz for both stage S2 (blue) and SWS (orange). Solid lines are the average traces in S2 and SWS, dotted lines show the SD about the means across all subjects. Note that both average amplitude (the value of the trace at time = 0) and time profile (the curve peaks about 0.5 seconds before and after the trough) are the same in the two sleep stages. (D) Density of SO in each sleep stage (average across all electrodes) is compared. Each square is a different subject. Note that SO density in SWS is higher than S2 in all subjects, and density in SWS correlates positively with density in S2 (Pearson's correlation $\rho = 0.57487$, $**p = 0.000376 < 0.001$). (E) The sample distribution of the ratio of SO density in SWS over S2. Note that if the ratio was the same across subjects the distribution would show symmetric tails at two sides of a mean peak. Instead, the sample distribution shows a large positive tail and a strong peak at the smallest value, indicators of an exponential-like distribution of ratios in the population. (F) Distribution of the average SO density found across all electrodes, shown in log-scale (using natural logarithm) to compare the two sleep stages. Consistent with D, the density is much higher in SWS for all electrodes, but within each stage it is clear from this plot that Frontal electrodes show a higher density than

hypothesized that when studying the detection of SOs at electrode pairs (a time-interval co-detection) we would find different groups of SOs, some co-detected at many electrodes in the same time window, and some with more localized co-detection. To inspect this hypothesis, we used a clustering algorithm to objectively organize the detected SO co-occurrences.

To prepare our data for analysis, for each detected SO event, we associated a binary (yes/no) array where each electrode that showed an SO trough within ± 400 ms of the detected trough was marked 1 (yes) and other electrodes were marked 0 (no). We used the ± 400 ms time range because in previous analysis [17] a quantified range of SO propagation was shown to be between 40 and 360 ms. Listing all these yes/no arrays next to each other built a SO co-detection matrix, and we constructed two separate matrices for the two sleep stages: one matrix contained a binary array for each SO detected during S2 in all subjects, and one the analog for SOs detected during SWS. Clustering separates a population of points in space, according to a chosen distance and selection parameters; k-clustering is optimized to minimize the distance between data points assigned to a cluster and its center of mass (its centroid). This algorithm (function *kmeans* in Matlab, The MathWorks) found three clusters, which we interpreted as Global, Local, and Frontal SO troughs, based on how their centroids were organized on the electrode manifold. The centroids for the clusters in the SO trough co-detection matrix during S2 and SWS are shown in Figure 2A: in both sleep states one centroid has all coordinates at zero, meaning no consistent co-occurrences could be placed on the electrode manifold, we labeled the SO troughs assigned to this cluster “Local”. Another centroid showed a majority of electrode coordinates at 1, we labeled these SO troughs “Global”. The last centroid shows nonzero coordinates only at frontal electrodes, thereby identifying as “Frontal”. Throughout the rest of the paper, we will refer to SO troughs belonging to each cluster as SO troughs of one “type”: Global, Local or Frontal. We call the number of electrodes in which an SO is detected within ± 400 ms its footprint. Across clusters, Local SOs had the smallest footprint (average 16.25% of electrodes during S2 and 20% during SWS), Frontal SOs had a slightly larger footprint (38.66% in S2, 34.62% in SWS) and Global SOs had the largest footprint (66% in S2, 63.93% in SWS), larger than the average footprint across all SOs grouped together (45.58% at S2, 41.89% at SWS).

Given the hypothesis [27] that neural oscillations related to sleep-dependent memory in S2 and SWS could be dissociated by global versus local cortical processing, respectively, we compared the fraction of SO troughs assigned to each cluster (Figure 2B), and found that though Global SO troughs were generally most abundant, visual inspection of the data showed marked differences in the pattern of probabilities in S2 and SWS, with greater Global SOs in S2 compared with SWS ($43.30 \pm 2.33\%$ and $36.28 \pm 1.81\%$ for S2 and SWS, respectively). Interestingly, this pattern was reversed in the Local cluster ($25.63 \pm 1.19\%$ in S2 and $34.66 \pm 1.47\%$ in SWS), while no differences appeared in the

Frontal cluster ($31.07 \pm 1.97\%$ and $29.06 \pm 1.47\%$ in S2 and SWS). We formally tested this hypothesis in a repeated measure analysis of variance (ANOVA) analysis to show possible sleep stage by SO type interaction (Figure 2B). Indeed, we found a stage-by-type interaction ($p < 0.001$) (the complete ANOVA and post hoc analysis are reported in Supplementary Tables S5 and S6). Post hoc comparisons with paired t-tests (Bonferroni-corrected significance at $p < 0.0033$) showed significantly more Global SOs in S2 than SWS, and the reverse case was also true that there were significantly more Local SOs in SWS compared with S2. We hypothesized that this Global-to-Local switch could be driven by a trade-off between Global SOs in S2 and Local SOs in SWS, so within the same post hoc analysis, we tested if there were cross-sleep-stage trade-offs in Global and Local SOs. Interestingly, we did not see (Supplementary Table S6) a significant difference between the fraction of Global SOs in S2 and Local SOs in SWS; however, the complementary result was highly significant that S2 contained far fewer Local SOs than Global SOs in SWS. Thus, our data are consistent with the hypothesis that S2 may involve more global processing compared to SWS. Interestingly, within an individual, we did not see a trade-off between the fraction of Global SOs in S2 and fraction of Local SOs in SWS. Instead, subjects who had a relatively larger fraction of Global SOs in S2 also showed a larger fraction on Global SOs in SWS. In fact, the fraction of Global SOs in S2 and SWS were significantly correlated (Figure 2C, Supplementary Figure S2), and intriguingly the fraction of Global SOs in one stage was negatively correlated to the fraction of Frontal SOs in the other stage (Figure 2C, Supplementary Figure S2). In support of our choice of three cluster labels, we found the average coordinate values of all SO troughs in each cluster and plotted in topoplots (Figure 2D), together with the grand average coordinates of all SO troughs on the delay-incidence matrix. It is evident that without clustering, the average SO trough appears localized at fronto-central electrodes, while clustering reveals the presence of the three different topographic types.

Since Global SOs were marked by a larger footprint on the electrode manifold, they represented events that were more synchronous across the whole scalp compared to Local or Frontal SOs. Because the degree of synchronization of cortical events could be tied to a generalized functional connectivity, which has been hypothesized to gradually decrease during sleep [34], we studied if the size of SO clusters were changed across the night. We binned the night in 2-hour-long bins and calculated the number of SOs in each cluster in a given time bin (separately for S2 and SWS). To allow comparison across subjects, we normalized the SO count in each cluster by the total number of SOs in the given sleep stage (Figure 2E). Our data showed that the fraction Global SOs within S2 was rather stable through the night, while Local and Frontal SOs during S2 slightly decreased in time. Conversely, in SWS we saw all fractions of SO types progressively decreasing through the night. Hence, our data did not show a larger fraction of Local SOs as the night

Figure 1. (Continued) Parietal and Occipital ones, in both sleep stages. (G) Comparison of SO density in SWS versus S2 at each electrode. Mean and standard error of the mean across subjects are shown for all electrodes. The list of electrodes starts frontally and ends occipitally, as indicated by Frontal, Central, Parietal, Occipital labels. Stars mark electrodes where SO density in SWS was significantly higher than in S2 (see Supplementary Tables S1–S3, repeated measures ANOVA and post hoc Wilcoxon signed rank test with Bonferroni correction). (H) Frontal electrodes in SWS show significantly higher SO density than other electrodes. For this statistical comparison, we grouped electrodes as shown in the left panel (F = Frontal, C = Central, P = Parietal, O = Occipital, L = Left Lateral, R = Right Lateral). Within each group, the average SO density and its standard error of the mean are shown in the barplot in the right panel, for SWS (orange) and S2 (blue). Stars show that when comparing SO density at frontal electrodes in SWS to SO density at other locations, it was significantly larger (see Supplementary Table S4, repeated measures ANOVA).

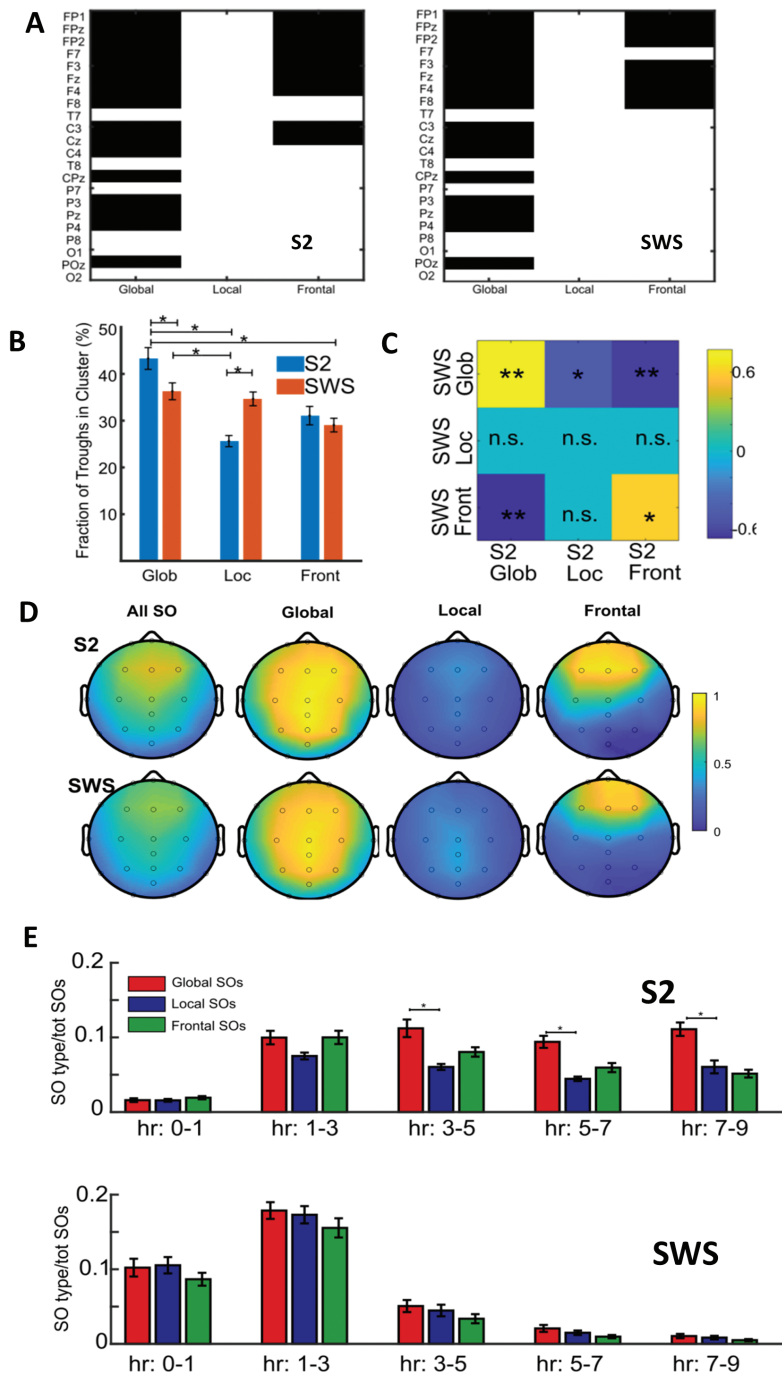


Figure 2. Clustering identifies Global and Local SOs in S2 and SWS, with differential distribution of the SO types across sleep stages. (A) Matrices of cluster centroid coordinates in S2 (left panel) and SWS (right panel), different columns represent different clusters. Because we used Hamming distance, the centroid coordinates have either 0 or 1 magnitude. Within a cluster, black marks an electrode which is present in the centroid (magnitude 1) while white shows an electrode which does not contribute to the centroid (magnitude 0). Clusters are marked as Global, Frontal, or Local according to which electrodes show nonzero magnitude in the centroid. (B) Comparison of the fraction of all detected SO troughs belonging to each cluster in S2 (blue bars) and SWS (orange bars). Error bars mark the standard error of the mean across subjects. Note that while the fraction of Global SO troughs diminishes from S2 to SWS, the fraction of Local SO troughs grows. Stars show the significant differences (repeated measures ANOVA, post hoc paired t-tests, *5% significance after Bonferroni correction, see [Supplementary Tables S5 and S6](#)). Note that while the fraction of Global SOs is significantly larger than the fraction of Local SOs in S2, it is not so in SWS. (C) Across subjects, correlation of cluster sizes across the two sleep stages (see [Supplementary Figure S2](#) for scattergrams of subject data). Pearson's correlation coefficients are in color in the matrix (see colorbar to the right), * $p < 0.005$, ** $p < 0.0001$ after Bonferroni significance correction at $0.05/9 = 0.0054$. (D) Considering all SO troughs belonging to each cluster, the relative presence of an electrode coordinate (i.e. detection of the SO trough at that electrode within ± 400 ms) is shown in topoplots, together with the "All SO" condition, meaning grouping all the SO troughs together rather than separating them in clusters. Note that when SO troughs are not clustered, the presence of electrodes matches the SO density At Detection ([Figure 1F](#)), but in separate clusters the signature of Global, Local, and Frontal SO troughs on the electrode manifold becomes evident. Top row: S2, bottom row: SWS. (E) Global/Local SOs cluster size changes in time. Fraction of SOs of a given type over all SOs in a sleep stage as the sleep night proceeds (x-axis shows hours of the sleep night considered). Mean and standard error of the mean across all subjects are reported. Statistical analysis of S2 (top plot) reported in [Supplementary Tables S7 and S8](#) (repeated measures ANOVA with post hoc analysis) and statistical analysis of SWS (bottom plot) in [Supplementary Table S9](#) (repeated measures ANOVA).

progresses; however, we found that the overall profile of SO type in time was not identical in S2 versus SWS: time had an effect on the Global and Local fractions in both sleep stages, but SO type drove different profiles only in SWS (Statistical analyses in [Supplementary Tables S7–S9](#)).

Once we confirmed that different trough types had different long delay incidence on the electrode manifold, we worked on further characterizing the three SO types. We first examined whether SO troughs of different types had different amplitudes (for information on SO amplitude before clustering, see [Supplementary Figure S3](#), where the relation between footprint and amplitude across electrodes before clustering is shown). [Figure 3A](#) shows the average of all SO troughs detected at electrode Fz during S2, separated by trough type (for the analogous figure in SWS, see [Supplementary Figure S4](#)). On average, Global SO troughs showed the largest amplitude at Fz. Next, we compared the amplitude of SO trough types across electrodes. In general ([Figure 3A](#) and [Supplementary Figure S4](#)) Global SOs had larger amplitudes than other types; however, the three SO types were the most separated in amplitude at frontal electrodes, where Global SO troughs were significantly larger than all others, and Local SO troughs were significantly smaller (statistical analyses in [Supplementary Tables S10–S13](#)). Note that the SO amplitudes were calculated in the signal filtered in the (0.5–1.5) Hz band, covering most of the duration of detected SO events ([Supplementary Figure S1](#)). To better visualize the topographical

selectivity of this amplitude difference, we re-plotted the averages from [Figure 3B](#) (as absolute values) in topoplots in [Figure 3C](#), which showed that Global SOs were largest (more than average) at F3-Fz-F4 electrodes, and Local SOs were smallest at frontal-to-central electrodes.

Global SOs spread in time

Given the characterization of Global SOs having high amplitudes at frontal electrodes, we tested the hypothesis that Global SOs would be initiated frontally and be detected progressively in time at central, parietal and occipital electrodes. To study this question, we built relative-detection probability curves for each possible pair of electrodes. Given an SO detection at one electrode, we found the probability that the other electrode in the pair also had an SO detection at a time delay (in a range of ± 400 ms, as before). We computed these curves for each SO cluster independently. The curves generally peaked around 0 delay, however when the topographical distance on the electrode pair was large, they occasionally looked a-symmetric about 0 delay. [Figure 4A](#) shows four examples of probability curves with the same zero-time electrode (Fz) and with second detection electrode progressively moving away from Fz ([Supplementary Figure S5](#) shows one example of the curves without clustering for a single subject and a single reference electrode). The multiple curves representing probabilities for different SO trough

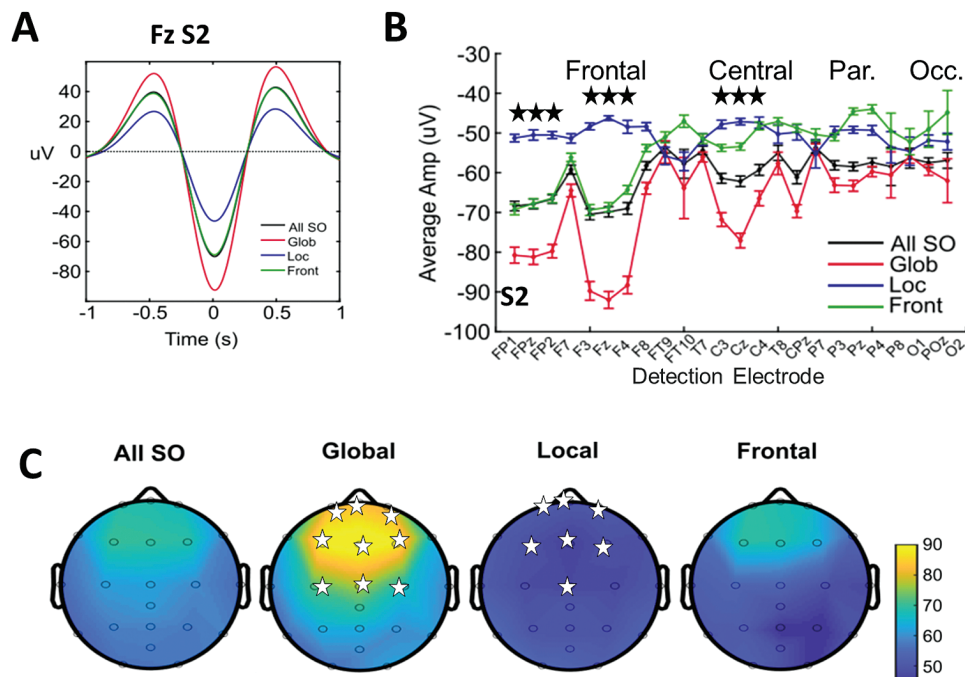


Figure 3. Global SO troughs have largest amplitude at frontal electrodes. (A) Average shape of SO detected at electrode Fz grouped within clusters, during S2. While the Frontal average SO matches the overall average SO trace without clustering (All SO), the average of Local SO has lower amplitude than All SO and the average of Global SO has higher amplitude (SWS case shown in [Supplementary Figure S4A](#)). (B) Average amplitude of SO troughs for separate clusters across all electrodes during S2 (SWS in [Supplementary Figure S4B](#)). Error bars show the standard error of the mean. Labels for the regions in which the detections electrodes are (Frontal, Central, Parietal, Occipital) are reported above the errorbars. Note that Global SO troughs have much larger amplitudes at frontal electrodes compared to all other SO troughs. Repeated measures ANOVA with 2 factors show an interaction of electrode-by-SO type in SO trough amplitude. Post hoc analysis with Wilcoxon signed-rank test show significantly larger SO trough amplitude for Global SOs at frontal electrodes compared to other SO types: *0.05 significance after Bonferroni correction ([Supplementary Tables S10–S13](#)). (C) Topoplots of the average amplitude of SO troughs by cluster. Comparing the clusters further emphasizes the frontal selectivity of Global SO troughs large amplitude. Stars in the Global SO topoplot mark electrodes where Global SO amplitude is significantly larger than Local SOs and Frontal SOs (same as panel B), stars in the Local SO topoplot mark electrodes where Local SO troughs have significantly smaller amplitude than Global and Frontal SOs (Post hoc analyses [Supplementary Tables S12 and S13](#)).

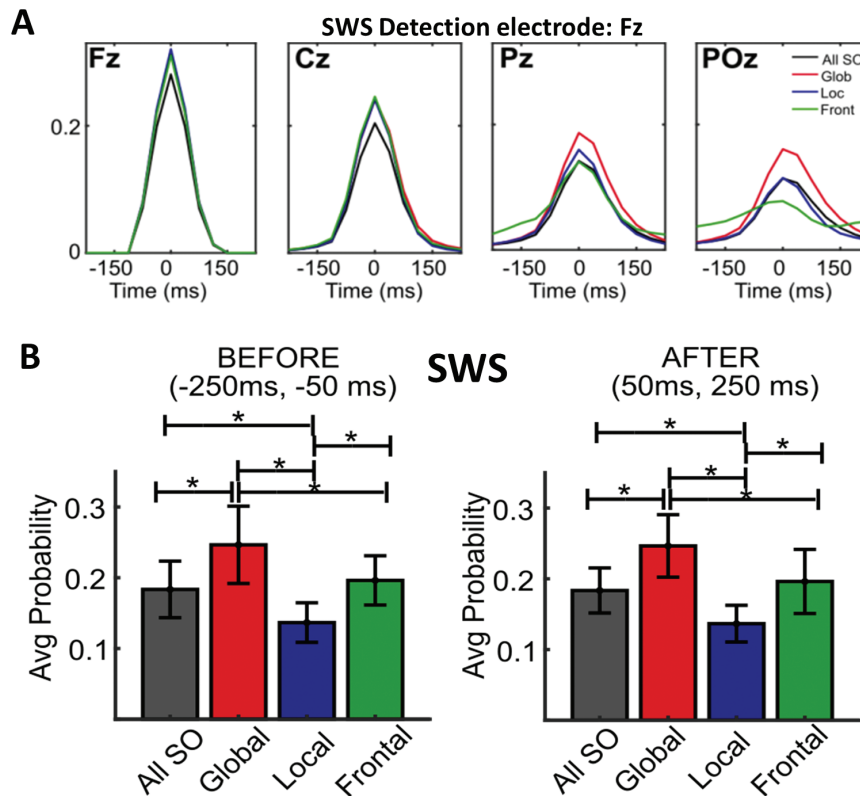


Figure 4. Global SOs have past and future on the electrode manifold. (A) Examples of the different probability of detection profiles when separating SOs by clusters (computed compounding all subjects). Given an SO trough is detected at electrode Fz, the probability detecting an SO trough at another electrode within a time range is shown (examples within SWS shown). For readability, we show curves that are Gaussian-smoothed fits of binned time-probability histograms. An example of raw histograms for one subject is reported in [Supplementary Figure S5](#). Note that as the distance between detection electrodes grows the curves show lower peaks (consistent with [Supplementary Figure S10](#)) and different clusters show different profiles. In particular, Global troughs show higher probability to detect an SO trough at parietal electrodes when one is found at Fz. (B) Two time ranges are chosen to investigate the probability of trough detection on the electrode manifold with a time lag: before (-250, -50) ms and after (50, 250) ms. For each time range, the area under each probability curve within the time range is found, and summed across all electrodes. The average across all detection reference electrodes is then reported in the bar plot, with standard error of the mean as error bars. The two plots are for SWS, the analogous bar plots for S2 showing consistent trends are shown in [Supplementary Figure S6](#). Significantly different probabilities are marked with * (ANOVAs followed by post hoc Multiple Comparisons tests. * $p < 0.05$ after Bonferroni correction for all possible pairs, see [Supplementary Tables S14–S17](#)). Even if with this calculation we remove all topographical details, it is still clear that Local SOs show very low probability of SO troughs detection in their past or future, while Global SOs show enhanced probability of detection of SO troughs at other electrodes in their past and future. This suggests that Global SOs could be traveling waves.

types all tended to peak at time zero, suggesting some degree of volume conduction might be at play. However, the curves across clusters became progressively different as the distance between zero-time and second electrode increased, hence showing that the process captured by these curves after clustering was not just passive conduction. Probability curves for Global troughs showed higher peaks, and broader tails, and curves for Frontal SO troughs grew increasingly asymmetric. This suggested that SOs of different types might show different topographies in time, hence show different spatio-temporal patterns.

To quantify the time-related differences between probability curves of different SO cluster types, we chose three time intervals: The “Before” interval at (-250, -50) ms, the “After” interval at (50, 250) ms and the “At Detection” interval at (-100, 100) ms. The intervals were chosen with a small overlap to avoid inserting edge effects in our comparisons. Looking at the probability curves within these intervals, we tested if SOs of different types had different topographies in time. Specifically, we found the area under the probability curve in each time range, separately for Global, Local, Frontal SOs as well as for all the SOs pooled together, to calculate the net probability that a given SO was related to another SO found in its past, or in its future.

We initially compared past and future probabilities across cluster types, and summed all the time-constrained probabilities across all the electrode pairs. As the bar plots in [Figure 4B](#) (and [Supplementary Figure S6](#)) show, Global SOs are the type most likely to show some relative detection at mid-to-large delay, both in the preceding and following time around the detection of a Global SO trough. At the opposite end, Local SOs showed the least probability that a detected SO will show a related detected SO at a different electrode in the considered delays (statistical analyses in [Supplementary Tables S14–S17](#)). Intuitively, we interpreted this result as showing that Global SOs had greater past and future history on the electrode manifold, while Local SO troughs show the least amount of history.

We next examined the topographical structure of the SO detection probability in time by considering one detection electrode at a time, and calculated the probability of detection in all electrodes in reference to the first detection electrode, across the three different time intervals. We constructed topoplots of the different probabilities across detection-reference electrodes ([Figure 5](#) and [Supplementary Figures S7–S9](#)). For a given detection-reference electrode, we show on different columns the probability computed for All SOs, Global SOs, Local

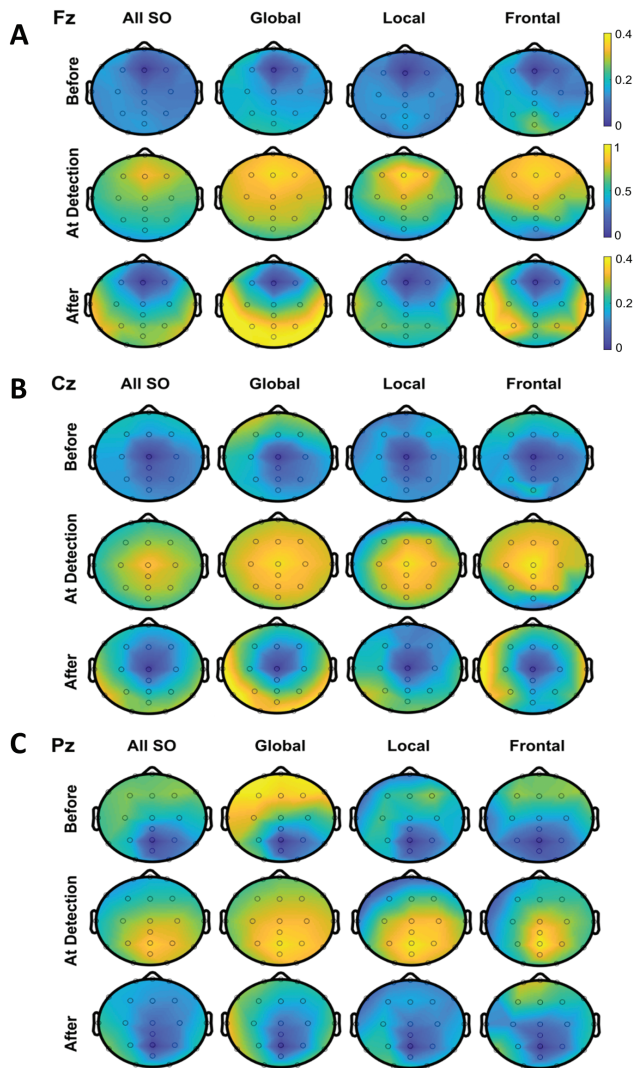


Figure 5. Only Global SOs show time-related topography: from frontal to occipital electrodes. (A) Topography of SO troughs detection (during SWS) within a time window around the detection of an SO trough at a fixed electrode (Fz). Each row shows a different time range: Before (−250, −50) ms, At Detection (−100, 100) ms and After (50, 250) ms. Each column compares SO troughs of different clusters, to show a time-cluster analysis of SO relative detection probability on the electrode manifold. Note that Global SOs have large probability After detection on the parieto-occipital region. (B) same as A but for detection at electrode Cz. (C) same as A but for detection at electrode Pz. Note that Global SOs have large probability Before detection on the fronto-central region. Supplementary figures show analogous profiles for detections at electrodes FPz and POz in SWS (Supplementary Figure S7) and in electrodes Fz-to-Pz during S2 (Supplementary Figure S8) and FPz and POz during S2 (Supplementary Figure S9).

SOs, and Frontal SOs. The top row shows the topography of the probability of detecting an SO before time-zero, while the middle row shows the present (around the time of detection) and the last row shows the topography of SO probability after detection at the time-zero electrode (Fz, Cz, and Pz during SWS for Figure 5 panels A, B and C, respectively). At detections, the plots show that SOs of all types had some nearest-neighbor co-detection topography, with Global SOs showing the largest footprint for the “At Detection” time interval (for topography of SOs for short and long time intervals around time 0, see Supplementary Figure S10). For time intervals before and after detection, the plots illustrate that Local SOs have in general no

clear topographical structure in their past or future probabilities (top and bottom rows), while Global SOs detected at frontal electrodes consistently showed a high probability of future SOs in the posterior-occipital electrodes. Conversely, Global SO troughs detected in more posterior electrodes showed a consistently high probability of SOs located at earlier times in frontal electrodes. Once again, when compared to Local SOs, those past/future preferential topographies disappeared. In addition, Frontal SOs behaved like the smaller versions of Global events, which showed a mild probability of a future detection toward lateral and occipital electrodes and a consistent past in frontal electrodes when detected more posteriorly.

We conclude that the population of all detected SOs on the electrode manifold does not show a unique dominant spatio-temporal behavior organized from frontal to posterior electrodes. Indeed, this structure seems to apply only to about 40–45% of the total SOs detected, which we call Global SOs. Frontal SOs resemble Global SOs in the fact that they have a past in frontal electrodes and a future in lateral/posterior electrodes but the probability values are smaller, and overall the topography emphasized their frontal dynamics over one extended to the whole electrode manifold. Finally, a third type of SO troughs, Local type, showed no special topography in the past or the future, and dynamics best described as locally emergent and short-spreading.

SO types and spindle/sigma activity

A strong prediction emerging from the Genzel model is that Global SOs should engage more system-wide thalamocortical features compared with the majority of Local SOs in sleep. Here, we asked if our different SO types resulted in a differential interaction with sigma power (12.5–16) Hz and spindles. We started by aligning sigma power at each electrode to SO troughs and averaging the relative change (z-scored, see methods for details). Figure 6A leftmost plots show the resulting profiles for stage S2 and SWS (bottom and top plot, respectively). In both plots there was a peak at positive time, indicating that indeed sigma power grew in the second following an SO trough, consistent with previous results [1, 35]. Dashed lines in these plots show the time ranges within which the sigma amplitude was modulated by the SO trough. To unpack this relationship on the whole electrode manifold, we re-calculated the same SO-aligned sigma plots separately for each electrode. Then, we calculated the average of each curve within the time ranges found in Figure 6A curve plots, indicating how much sigma power was found after an SO trough at each electrode. This average z-score was calculated both including all SO cluster types together, and separating the SOs of different types. The resulting SO-aligned average sigma power (z-scored) is shown in topoplots in Figure 6A. The top row refers to sleep stage S2, the bottom row to SWS. As can be seen by the topoplots labeled “All SO”, Sigma power does grow in relation to SO troughs at all electrodes on average, and this property remains true when only Global SOs are considered, in both S2 and SWS. In the case of Frontal SOs, this modulation of sigma power after SO trough is only visible at fronto-central electrodes in both stages. For Local SOs, the amplitude growth is practically absent during S2 and present only at posterior location during SWS. To better quantify these comparisons, we grouped Frontal, Central and Parieto-occipital electrodes (Figure 6B, inset) and compared the average sigma amplitude across these locations

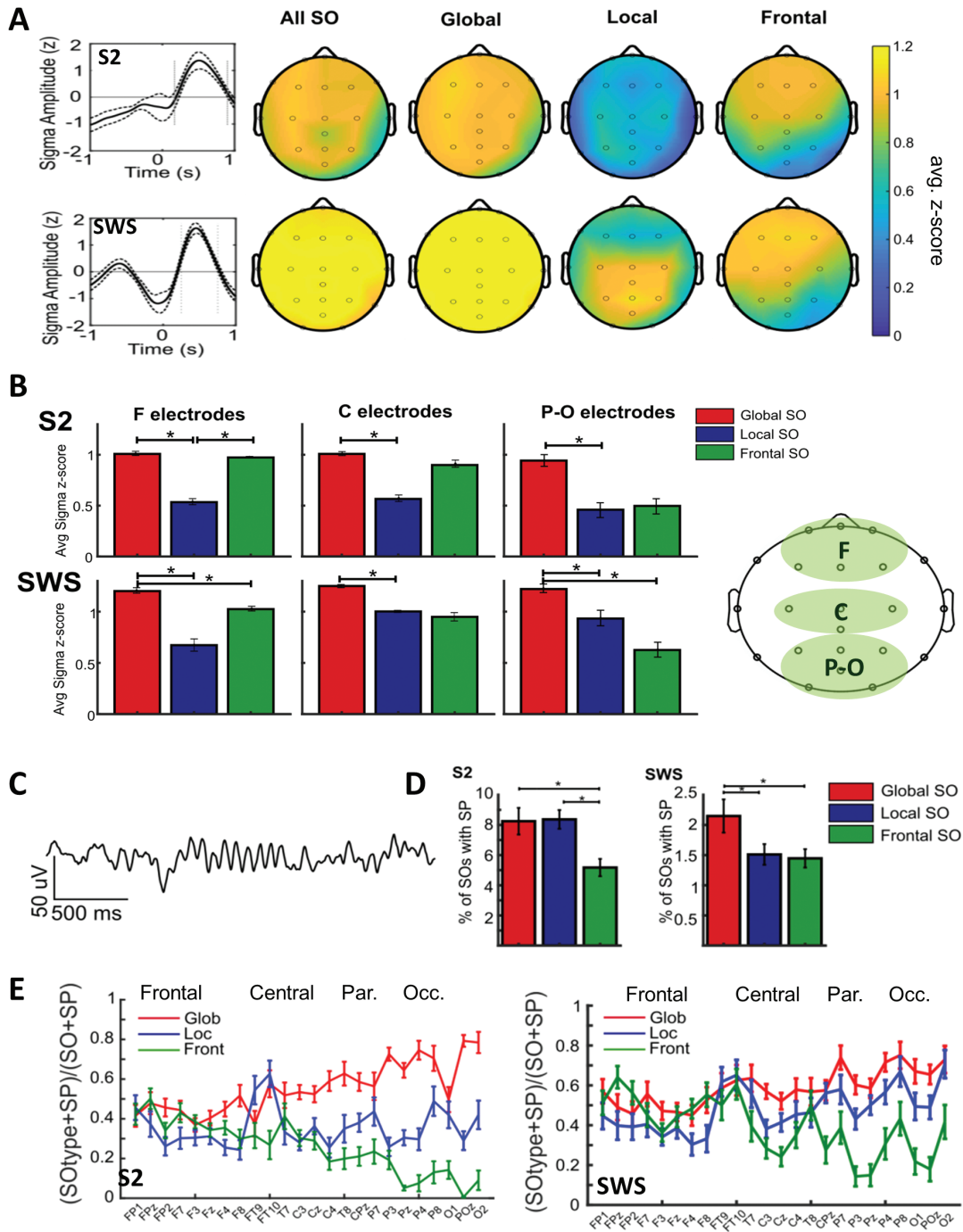


Figure 6. Fast spindles are preferentially detected after Global SO troughs. (A) Average fast sigma amplitude (z-scored) aligned to SO troughs in S2 (top row) and SWS (bottom row). Dotted lines show the time range used to find the average z-Amplitude under the peak, shown in the first (leftmost) topoplot (All SO). The same estimate is repeated considering SOs of each cluster separately. Note that Global SOs show a large increase in fast sigma amplitude, while Local SOs show a much smaller increase, for both S2 and SWS. (B) Comparison with statistical analysis across locations on the electrode manifold of z-scored sigma amplitudes (average and standard error of the mean across the grouped electrodes) aligned to SO troughs of different types. The right topoplot shows which electrodes are averaged in the Frontal (“F electrodes”), Central (“C electrodes”) and parieto-occipital (“P-O electrodes”) groups. Two sleep stages separately considered: S2 (top row) and SWS (bottom row). Comparisons between sigma amplitude aligned to SOs of different types were conducted with pairwise *t*-tests, with Bonferroni correction for multiple comparisons (*p* < 0.05 after Bonferroni correction, see [Supplementary Table S18](#)). (C) One example of detected spindle in electrode CPz during stage S2 of one subject. Note that the channel trace includes about 1 second before and after the spindle event. (D) For SOs of different clusters, the percent of SOs of that type in the given sleep stage which show a fast spindle near the SO trough (i.e. in the time cycle between begin and end of the SO event) is shown. For each subject, this percent is averages across all electrodes, and shown in bars is the mean and standard error of the mean across all subjects, for stage S2 (left panel) and SWS (right panel). Stars (*) mark statistically different means according to Wilcoxon signed rank test after Bonferroni correction for multiple comparisons ([Supplementary Table S19](#)). (E) Relative contribution of different clusters to the probability of detecting a fast spindle after an SO trough. At each electrode, we show the ratio between the count of SOs of a type that are paired to a spindle over all SOs that are paired to a spindle. The ratio is shown in the errorbars as mean and standard error of the mean across subjects, and gives the sample probability that SOs paired to a spindle belong to a given cluster. Stage S2 (left plot) and SWS (right plot) shown separately. Repeated measures ANOVA with two factors show an effect of SO type and interaction of SO type and electrode in S2, and an effect of SO type, electrode and interaction in SWS ([Supplementary Tables S20–S22](#)).

(Figure 6B). Statistical analysis (Supplementary Table S18) showed that during both S2 and SWS Local SOs had significantly less high sigma peaks associated, compared to Global SOs, at all topographic locations, while Frontal SOs had sigma peaks comparable with Global SOs at Frontal locations in both sleep stages.

Since we found that sigma power interacted differently with each SO type, we hypothesized that also the detection of sleep spindle events in relation to SO troughs would look different across SO types. For each electrode, we applied a spindle detection algorithm based on work by Wamsley [31] and Wendt [36], and marked the peak of each spindle event (Figure 6C shows one example spindle detected). Then, for each SO trough detected at one electrode, we estimated the probability that a spindle was detected at the same electrode during the SO event around the trough, and we repeated this estimate using only SOs of each type. Figure 6D shows the fraction of SOs of any given type that did show a spindle associated with them. About 8% of all Global SOs and 8% of all Local SOs showed a paired spindle in S2, and only 2% of Global SOs and 1.5% percent of Local SOs were paired to a spindle at the electrode during SWS (statistical analysis in Supplementary Table S19).

To complete the picture of the spindle-SO occurrence probability, we also calculated the probability that, given a spindle/SO complex was detected, what was the SO type (Global, Local or Frontal)? We calculated these probabilities separately for each electrode, and their averages across all subjects were compared in Figure 6E (left plot for S2, and right plot for SWS). For detection at frontal electrodes, the relation to spindle detection was similar across the different SO types. In centro-parietal electrodes, Global SOs showed a much stronger relation to spindle detection than any other SO cluster type, especially in S2, as can be seen comparing the heights of the bars of different color within

each electrode plot of Figure 6E. This was especially interesting, because the centro-parietal region of the electrode manifold is where the majority of spindles are typically detected [37] (note that since this is a ratio, the resulting bar heights are normalized by the relative amount of SO-spindles pairs detected at different electrodes). We tested if the different bar heights in Figure 6E resulted in statistically significantly different probabilities and found an effect of SO type and interaction of SO type and electrode in S2, and an effect of SO type, electrode and interaction in SWS on the fraction of SO of a type which showed a time relation to spindles (Supplementary Tables S20–S22).

In light of this enhanced interaction between spindles and Global SO troughs, we asked if this resulted in a stronger coordination of SO (0.5–1.5 Hz) and sigma (12.5–16 Hz) activity, which we quantified using the MI introduced by Canolty et al. [33]. In our case, we used MI to quantify the degree to which the phase of SOs affected the amplitude of sigma oscillations. Note that since we are using the SO band to find the phase of SO oscillations, we were careful to consider a narrow band around the average frequency of SOs, thus enhancing the chance of getting a correct fit to data when using Hilbert transform to estimate the phase. To distinguish MI for the different SO types, we only calculated the phase-amplitude modulation in short time epochs around the detection of SO troughs, separated by SO type. As a result, higher MI for a given SO type would indicate that the effect of SO phase on sigma amplitude is stronger for that SO type. In Figure 7A, we compare MI (average across subjects) among the three SO cluster types. In light of the topographical differences present in the spindle detection probabilities (Figure 6E), we compared the delta-sigma phase-amplitude modulation indices for each electrode separately. Comparing different SO types within each electrode, the bar plots show that for frontal electrodes the strong

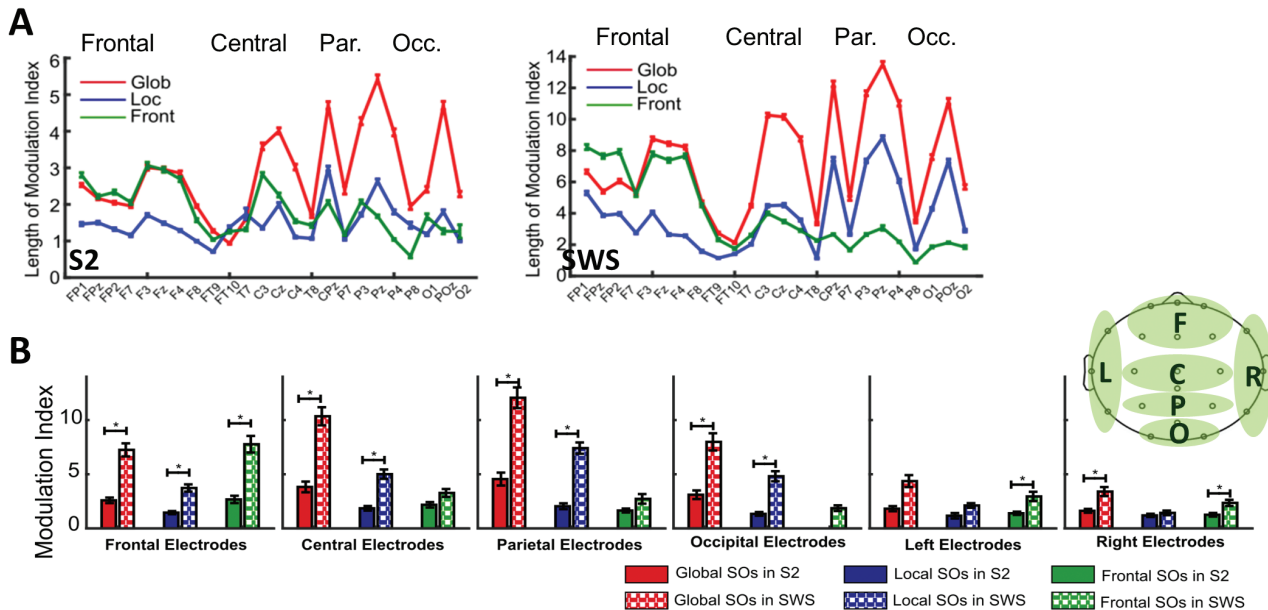


Figure 7. SO-sigma phase-amplitude modulation is stronger for Global SOs. (A) For each electrode, the normalized phase amplitude modulation vector length (MI, range 0 to 40) is calculated around SOs, separated by cluster. Errorbars show the average across subjects and standard error. For S2 (in left panel) ANOVA showed an effect of Electrode, SO cluster and Electrode-by-Cluster interaction. Analogously, for SWS (right panel) repeated measures ANOVA showed an effect of Electrode, SO cluster and Electrode-by-Cluster interaction (Supplementary Tables S23 and S24). (B) MI across sleep stages, SO type and electrode locations. Electrodes were grouped by location (see inset) and MI values are shown as mean and standard error of the mean across subjects. ANOVA showed an effect of Electrode location, an effect of SO cluster, and effect of sleep stage and all interactions (Supplementary Table S25). Post hoc analysis with Wilcoxon signed rank test was conducted to compare for different sleep stages, $^*p < 0.05$ after Bonferroni correction (Supplementary Table S26).

phase-amplitude modulation between SO and sigma oscillations was mediated by Global and Frontal SOs, while for centro-parietal and occipital electrodes the modulation was strongest for Global SOs only. When comparing across electrodes, our data also showed a small increase in MI values for Global SOs from frontal to centro-parietal electrodes, from slightly below 10 frontally to slightly above 10 centro-parietally in SWS. This difference was likely due to known larger sigma power peaks found at C-P electrodes compared to frontal electrodes [37]. Nonetheless, if the larger sigma power was the only factor inducing larger MI values that would apply uniformly to the MI values of all types, hence we concluded that the relative dominance of Global SOs on the SO-sigma phase amplitude modulation at C-P electrodes was present in our data. In fact, with statistical comparisons (Supplementary Tables S23 and S24) we found an effect of electrode, of SO type and of SO type-by-electrode interaction in the MI profiles, both in S2 and SWS.

When comparing the MI relating Global SOs to sigma across the two sleep stages, we chose to group electrodes across the scalp, in Frontal, Central, Parietal, Occipital, Left, and Right electrodes, to be able to conduct a comparison across multiple factors (see Figure 7B inset panel for a representation of the grouped electrodes). We found that the MI was generally higher during SWS (patterned bars in Figure 7B) compared to S2 (solid color bars in Figure 7B). Statistical analysis confirmed that (Supplementary Tables S25 and S26). In other words, going from light to deep sleep introduces an overall decrease in the fraction of Global SOs available, but an increase in their coordination with spindles and sigma. Together, these results support the prediction of greater thalamocortical modulation of brain activity during Global SOs, compared with other SO types.

Discussion

Our study introduces a new approach to studying the spatio-temporal occurrence of sleep oscillations on the electrode manifold, which enables the objective classification of SOs with respect to their co-detection across the whole electrode manifold. Our analysis revealed that SO clusters had clear topographies, with Global SOs involving almost all electrodes, Local SOs not having any specific location preference, and Frontal SOs confined to the frontal region. Global SOs were characterized by larger amplitude at frontal electrodes compared to other SO types. Our time-space analysis of the clusters showed that Global SOs had the highest probability of a past and a future, while Local SOs had the least. Clustering also allowed for the study of the interaction between SO and sigma oscillations (one possible cross-frequency coupling) separately for different SO types. Global SOs showed the strongest coordination with sigma power and spindles, compared to other SO types, with: (1) higher modulation of sigma power after a Global SO trough, (2) stronger probability that if a spindle is found coupled to an SO trough, that the SO was Global, and (3) higher SO-sigma phase-amplitude modulation (as measured by the normalized MI [33]). Thus, Global SOs appear poised to activate systems consolidation processes to a greater extent, compared with the other SO types. However, our analysis also showed similar interactions between sigma/spindles with Frontal and Global SOs—such that a combined 70% of all SOs localized to the frontal part of the scalp interacted with spindles.

We studied stages S2 and SWS separately, to compare how the Global/Local SOs were organized in the two sleep stages, in light of the hypothesis [27] associating S2 to global reorganization of synaptic architecture while more local activity during SWS could mediate overall homeostatic changes in connectivity [26, 28]. We found a significantly larger amount of Global SOs compared to Local during S2, and similar fractions of Global and Local SOs during SWS. In fact, the number of Global SOs significantly decreased from S2 to SWS, and vice-versa the number of Local SOs significantly increased from S2 to SWS. This supports the idea that global activity (in our case Global SOs) is markedly dominant in S2 sleep. However, the coordination of Global SOs and sigma power measured with the MI was much higher in SWS compared to S2. Therefore, while Global SOs are relatively less prevalent in SWS, they show a much stronger interaction with spindles. It is hence possible that oscillation-mediated processing during the two stages is indeed remarkably different: In S2, Global SOs are dominant but coordinate less strongly with spindles, while in SWS Local and Global SOs have similar incidence, but the Global events are highly linked to spindles. Future studies should investigate if this differential ability of Global SOs to coordinate nested oscillations (less in S2 and more in SWS) generalizes to other neural oscillations including sharp-wave ripples. In addition, there may be functional differences between Global SOs that coordinate spindles in SWS versus Global SOs that do not coordinate spindles in S2, which may impact memory consolidation.

In this work, we consider each SO as an event detected at one electrode, rather than an event occurring at multiple electrodes. This allows us to define a robust clustering algorithm that does not operate on manually biased data, and to run comparisons across electrodes of the SOs belonging to different clusters. In particular, it is important to note that when the relation between SOs and sigma are evaluated, the sigma signal and the spindles that each SO event is related to are detected at one electrode, once again constructing a within-electrode analysis that then can be compared across electrodes. In interpreting this data to build our understanding of the SO phenomena across the EEG manifold, one should note that the ratio of Global-to-Local SO counts could be slightly different if SOs are not counted as one event-by-electrode but rather as one overall “wave” detected on the whole EEG manifold. However, such interpretation will lead to events that are hard-to-quantify and manually define, as such hindering the reproducibility of the clustering procedure.

In this study, we found that the number of SOs found during one night of sleep in a single subject was not large enough to perform successful clustering analysis within each subject. Thus, we performed the cluster procedure on the combined dataset of all subjects rather than separately within subjects, which limits our ability to connect the clusters in one subject to functional outcomes, such as memory performance. In a study where multiple nights per subjects are collected, it would be possible to conduct clustering within subjects, enabling the study of individual differences in memory performance profiles in relation to Global/Local SOs. Furthermore, the intriguing result that SO density in the two stages was correlated, but with a non-constant ratio across subjects, suggests that SO-mediated processing during S2 and SWS could be connected, and hence related to learning. However, it is important to consider that SO density in nighttime sleep could be a trait characteristic [38, 39], perhaps modulated by gender and/or age differences. To dissect

these two possibilities (state-dependent learning vs. individual trait), multiple nights of sleep should be analyzed for a pool of subjects, to establish if the ratio of SWS/S2 density is constant in time within a subject or related to learning profiles.

In the past, SO topography has been studied through phase gradients [17] and recently the possible differences introduced by referencing to frontally detected SOs versus posteriorly detected SOs has been emphasized in a frequency-coupling context [21]. Recent work [24] classified SOs in two main types, and found relative predominance of smaller SOs later in the night, which is not consistent with our results if one interprets their smaller SO type to match our Local SOs. However, because of strong differences on how the analysis is conducted in our clustering approach compared to their separation criteria (SO detection averaging across the whole scalp, the collection of S2 and SWS SOs, choice of only two sleep cycles) it seems possible that their analysis was dominated by Global SOs (indeed the topography of the two types followed closely the average density topography that we saw before clustering) and their analysis suggest that there could be sub-types of Global SOs, with relatively subtly different interaction with spindles. Future studies could address within-cluster SO properties in relation to other brain oscillations.

Clustering showed that many SOs detected on the EEG are non-Global (either Frontal or Local). Research by Nir et al. [19] found a majority of nonsynchronous SO events when studying synchronous scalp and in-depth recordings of human sleep, also finding an overall reduction of SO footprints between early and late sleep. In our clusters, we did see that Global SOs were less than half of all SOs, but we did not see a trend of increased Local SOs in late sleep versus early sleep. Importantly, it is not clear how the notion of activating a large fraction of in-depth electrodes (a global event for Nir et al.) relates to our Frontal, Local, Global events on the EEG electrode manifold. Also, our notion of Global SOs allowed for 400 ms relative delay across electrodes, choosing a rather inclusive timing to allow for frontal-occipital traveling waves to be represented fully in our binary matrix.

In our work, we find a relation of fast spindles (and fast sigma band) with SOs that is consistent with previous results [35, 40] and we show that local and frontal SOs have less coordination with spindles than other SO types. The mechanism through which this coordination could be mediating memory consolidation is still unknown. Hypotheses include many variations on the theme of synchronized memory replay across brain regions that would induce specifically timed synaptic plasticity: whether because cortical oscillations guarantee such synchrony in localized population of cells [12, 41, 42] or because generalized synaptic rescaling weeds out synapses that were not strongly recently reinforced by behavior [34], or most recently a combination of the two [27]. While our data shows that indeed sleep memory processing as mediated by SOs is different in S2 compared to SWS, specific investigations should be conducted into the biophysical mechanisms that enable Global SOs coordination with sigma and limit the coordination of Local SOs with sigma, and whether coordinated and non-coordinated SOs have different roles in sleep-dependent consolidation.

Our clustering approach can be extended to other EEG oscillations that can be detected at single electrodes independently, such as sleep spindles and theta bursts. In fact, spindles topography on the electrode manifold is known to be variable [37, 43],

and it has been hypothesized that spindles could be originated in the core or matrix thalamocortical loops, with core spindles showing smaller footprint and less central topography, matrix spindles with intermediate footprint and central topography and mixed spindles (resulting from coordinated matrix-core activity) showing the largest footprint (perhaps global on the electrode manifold) [43]. Applying our clustering approach to sleep spindles could introduce explicit quantifiers over this variability, possibly identifying how many spindles can be considered core spindles, or matrix or mixed during a night of sleep. Furthermore, a clustering over independent detections approach applied to SO-spindle complexes would help to quantify the relative incidence of such coordination in a night of sleep. Broad use of this approach could begin to reconcile the possible complementary roles for brain-wide coordinated oscillations and more localized processing by revealing their relative incidence and time-space profiles.

Our results suggest a direct functional hypothesis on the mechanisms through which sleep interventions might improve SO-sigma coordination. The coordination between spindles and SOs, as mediated by SO-sigma phase-amplitude modulation, is often considered a possible proxy for memory processing during sleep [1, 2, 6, 44]. If that was the case, our data suggests that such processing is strongly mediated by Global SOs across the cortex, and possibly mediated by Global and Frontal SOs when processing is localized in the frontal regions. In line with this interpretation, interventions aiming to improve sleep-dependent memory consolidation through the enhancement of spindle-SO interaction, like noninvasive electrical stimulation—should be successful when promoting larger amplitudes of frontally detected SOs, since that would likely lead to a larger presence of Global SO events, and greater systems-level coordination with sleep spindles.

Supplementary Material

Supplementary material is available at SLEEP online.

Acknowledgments

The authors would like to thank Nicholas Reihanabad for sleep scoring about 50% of the subjects, and Dr. Mohsen Naji for sharing his code for initial detection of slow oscillations and spindles.

Funding

This work was supported by National Institutes of Health (NIH) grant (R01 AG046646) to S.C.M.

Conflict of interest statement. None declared.

References

1. Mölle M, et al. Slow oscillations orchestrating fast oscillations and memory consolidation. *Prog Brain Res.* 2011;193:93–110.
2. Diekelmann S. Sleep for cognitive enhancement. *Front Syst Neurosci.* 2014;8:46.
3. Novitskaya Y, et al. Ripple-triggered stimulation of the locus coeruleus during post-learning sleep disrupts ripple/

- spindle coupling and impairs memory consolidation. *Learn Mem.* 2016;**23**(5):238–248.
4. Latchoumane CV, et al. Thalamic spindles promote memory formation during sleep through triple phase-locking of cortical, thalamic, and hippocampal rhythms. *Neuron.* 2017;**95**(2):424–435.e6.
 5. Ladenbauer J, et al. Promoting sleep oscillations and their functional coupling by transcranial stimulation enhances memory consolidation in mild cognitive impairment. *J Neurosci.* 2017;**37**(30):7111–7124.
 6. Demanuele C, et al. Coordination of slow waves with sleep spindles predicts sleep-dependent memory consolidation in schizophrenia. *Sleep.* 2017; **40**(1).
 7. Girardeau G, et al. Selective suppression of hippocampal ripples impairs spatial memory. *Nat Neurosci.* 2009;**12**(10):1222–1223.
 8. Rasch B, et al. About sleep's role in memory. *Physiol Rev.* 2013;**93**(2):681–766.
 9. Sirota A, et al. Communication between neocortex and hippocampus during sleep in rodents. *Proc Natl Acad Sci U S A.* 2003;**100**(4):2065–2069.
 10. Staresina BP, et al. Hierarchical nesting of slow oscillations, spindles and ripples in the human hippocampus during sleep. *Nat Neurosci.* 2015;**18**(11):1679–1686.
 11. Latchoumane CV, et al. Thalamic spindles promote memory formation during sleep through triple phase-locking of cortical, thalamic, and hippocampal rhythms. *Neuron.* 2017;**95**(2):424–435.e6.
 12. Mehta MR. Cortico-hippocampal interaction during up-down states and memory consolidation. *Nat Neurosci.* 2007;**10**(1):13–15.
 13. Steriade M, et al. Cholinergic and noradrenergic modulation of the slow (approximately 0.3 Hz) oscillation in neocortical cells. *J Neurophysiol.* 1993;**70**(4):1385–1400.
 14. Steriade M, et al. A novel slow (< 1 Hz) oscillation of neocortical neurons in vivo: depolarizing and hyperpolarizing components. *J Neurosci.* 1993;**13**(8):3252–3265.
 15. Contreras D, et al. Mechanisms of long-lasting hyperpolarizations underlying slow sleep oscillations in cat corticothalamic networks. *J Physiol.* 1996;**494**(Pt 1):251–264.
 16. Timofeev I, et al. Origin of slow cortical oscillations in deafferented cortical slabs. *Cereb Cortex.* 2000;**10**(12):1185–1199.
 17. Massimini M, et al. The sleep slow oscillation as a traveling wave. *J Neurosci.* 2004;**24**(31):6862–6870.
 18. Volgushev M, et al. Precise long-range synchronization of activity and silence in neocortical neurons during slow-wave oscillations [corrected]. *J Neurosci.* 2006;**26**(21):5665–5672.
 19. Nir Y, et al. Regional slow waves and spindles in human sleep. *Neuron.* 2011;**70**(1):153–169.
 20. Ngo HV, et al. Induction of slow oscillations by rhythmic acoustic stimulation. *J Sleep Res.* 2013;**22**(1):22–31.
 21. Cox R, et al. Slow oscillations during sleep coordinate inter-regional communication in cortical networks. *J Neurosci.* 2014;**34**(50):16890–16901.
 22. Neske GT. The slow oscillation in cortical and thalamic networks: mechanisms and functions. *Front Neural Circuits.* 2015;**9**:88.
 23. Siclari F, et al. Local aspects of sleep and wakefulness. *Curr Opin Neurobiol.* 2017;**44**:222–227.
 24. Bernardi G, et al. Local and widespread slow waves in stable nrem sleep: evidence for distinct regulation mechanisms. *Front Hum Neurosci.* 2018;**12**:248.
 25. Murphy M, et al. The cortical topography of local sleep. *Curr Top Med Chem.* 2011;**11**(19):2438–2446.
 26. Tsai PJ, et al. Local awakening: regional reorganizations of brain oscillations after sleep. *Neuroimage.* 2014;**102**(Pt 2):894–903.
 27. Genzel L, et al. Light sleep versus slow wave sleep in memory consolidation: a question of global versus local processes? *Trends Neurosci.* 2014;**37**(1):10–19.
 28. Piantoni G, et al. Memory traces of long-range coordinated oscillations in the sleeping human brain. *Hum Brain Mapp.* 2015;**36**(1):67–84.
 29. *topoplot.m* [computer program]. <https://github.com/jukka/eeglab/blob/master/functions/sigprofunc/topoplot.m2001>. Accessed October 9, 2017.
 30. Dang-Vu TT, et al. Spontaneous neural activity during human slow wave sleep. *Proc Natl Acad Sci U S A.* 2008;**105**(39):15160–15165.
 31. Wamsley EJ, et al. Reduced sleep spindles and spindle coherence in schizophrenia: mechanisms of impaired memory consolidation? *Biol Psychiatry.* 2012;**71**(2):154–161.
 32. Sattari N, et al. The effect of sex and menstrual phase on memory formation during a nap. *Neurobiol Learn Mem.* 2017;**145**:119–128.
 33. Canolty RT, et al. High gamma power is phase-locked to theta oscillations in human neocortex. *Science.* 2006;**313**(5793):1626–1628.
 34. Tononi G, et al. Sleep function and synaptic homeostasis. *Sleep Med Rev.* 2006;**10**(1):49–62.
 35. Klinzing JG, et al. Spindle activity phase-locked to sleep slow oscillations. *Neuroimage.* 2016;**134**:607–616.
 36. Wendt SL, et al. Validation of a novel automatic sleep spindle detector with high performance during sleep in middle aged subjects. *Conf Proc IEEE Eng Med Biol Soc.* 2012;**2012**:4250–4253.
 37. Cox R, et al. Individual differences in frequency and topography of slow and fast sleep spindles. *Front Hum Neurosci.* 2017;**11**:433.
 38. Piantoni G, et al. Individual differences in white matter diffusion affect sleep oscillations. *J Neurosci.* 2013;**33**(1):227–233.
 39. Bódizs R, et al. Prediction of general mental ability based on neural oscillation measures of sleep. *J Sleep Res.* 2005;**14**(3):285–292.
 40. Andrillon T, et al. Sleep spindles in humans: insights from intracranial EEG and unit recordings. *J Neurosci.* 2011;**31**(49):17821–17834.
 41. Sirota A, et al. Interaction between neocortical and hippocampal networks via slow oscillations. *Thalamus Relat Syst.* 2005;**3**(4):245–259.
 42. Wei Y, et al. *Synaptic mechanisms of memory consolidation during NREM sleep.* Society for Neuroscience. San Diego, CA: Society for Neuroscience; 2016.
 43. Piantoni G, et al. The contribution of thalamocortical core and matrix pathways to sleep spindles. *Neural Plast.* 2016;**2016**:3024342.
 44. Cox R, et al. Involvement of spindles in memory consolidation is slow wave sleep-specific. *Learn Mem.* 2012;**19**(7):264–267.